2014 International Conference on Unmanned Aircraft Systems (ICUAS)
May 27-30, 2014. Orlando, FL, USA

Aerodynamic Sectional Modeling with the use of Extended Vectors

Ernesto Olguín-Díaz and Miguel A. García-Terán

Robotics and Advanced Manufacturing Group, CINVESTAV, Mexico,
ernesto.olguin@cinvestav.edu.mx, angelteran30@gmail.com

***Abstract*—This paper presents the dynamic model of an Unmanned Aerial Vehicle (UAV), specifically, a fixed-wing aircraft PT-40, using extended vectors in $\mathbb{R}^6$. This representation of cartesian coordinates in the Euclidian space simplifies the representation of the model to express each term in a single six dimensional vectorial equation, instead of the three dimensional, conventional linear and angular movement equations. The algebra to manipulate these elements reduces the number of operations and defines the basic transformations between the reference frames.**

The UAV is a free rigid body in $\mathbb{R}^3$ subject to aerodynamic forces, which are included in the model as exogenous forces. Typically these forces are calculated using dimensionless coefficients that capture the geometric complexity of the aircraft in the Aerodynamic Center of Pressure, resulting in a model with lumped aerodynamic parameters. Due to the advantages of the extended vectors, the aerodynamic forces acting on each component of the aircraft can be included in the mathematical model as independent effects.

***Keywords*—Aerial Robotics, Unmanned Aerial Vehicle, Multibody Modeling, Extended Vectors,**

I. Introduction

UAVs have a wide field of applications in areas like surveillance, rescue, military, reconnaissance and research. These areas require specific capabilities in UAVs, for example developing different kinds of flights under perturbation forces. In order to improve the behavior of these vehicles, morphing designs and new control techniques have been reported [1], [2], [3], [4]. In all these cases the dynamic model is very important, as well as for the design of aircraft and tuning controller gains.

Movements that are performed by small or natural scale airplanes are defined by the solution of 12 nonlinear ordinary differential equations [5], [6]. The rate of change of movement variables is defined by external forces and moments (gravity, control surfaces and wind). It is noteworthy that the behavior of any aircraft vehicle depends on the aerodynamic forces and moments and thus on the aerodynamic coefficients and accuracy with which they are calculated.

The total Aerodynamic effects are defined by Roscam in [7] as the sum of forces and moments which act on each component of the airplane, but these are commonly represented as a function of a set of lumped dimensionless coefficients. The differential equations are reduced and decoupled for defining the modes of aircraft motions (longitudinal and lateral-directional motions), which are used to analyze the stability and design the Controller [1], although working with this number of equations is complicated.

A common procedure to simplify the estimate of the aerodynamic coefficients is to neglect the effects which do not represent a significant contribution when the complete geometry of the aircraft is analyzed as a whole body. However, this consideration means that important effects are neglected, especially in the design of either ultra lightweight UAVs or micro UAVs. In [8] a generic nonlinear model of reduced scale UAVs is presented, where the dynamic model is reduced by neglecting the aerodynamic forces produced by the angular velocity vector. These procedures simplify the design of Controllers. However it is important to mention that the Controller has to be either robust in order to compensate the terms that were neglected or control the conditions of the experimental test.

The design of a solar UAV is presented in [9] by Noth, who presents an aerodynamic analysis on each component and the total aerodynamic forces and moments, as presented by Roscam in [7], are the sum of forces and moments in the center of mass. This concept is used by Paranjape in [10] where the wing of a tailless UAV is sectioned into two components and articulated, where the dihedral angle is modified independently on each section in order to change the total aerodynamic effects. The dynamic model in $\mathbb{R}^3$ is used to design a Controller [4].

On the other hand, Featherstone in [11] defined the spatial vectors (six-dimensional vectors) as a mathematic term that is defined by a pair of vectors $(\boldsymbol{a}, \boldsymbol{b}) \in \mathbb{R}^3$ in the 3-D Euclidian space, where $\boldsymbol{a}$ is a linear vector and $\boldsymbol{b}$ is a free vector. In the present paper we refer to a spatial vector as an extended vector. These vectors reduce the number of algebraic operations used to obtain the mathematical model of dynamic systems. The extended vectors are very often used in robotic systems to represent Kinematic and dynamic operations. Featherstone in [11] states that there are different kinds of extended vectors that have different physical and mathematical meanings. Some of these vectors will be defined in the modelling section.

978-1-4799-2376-2/14/$31.00 ©2014 IEEE

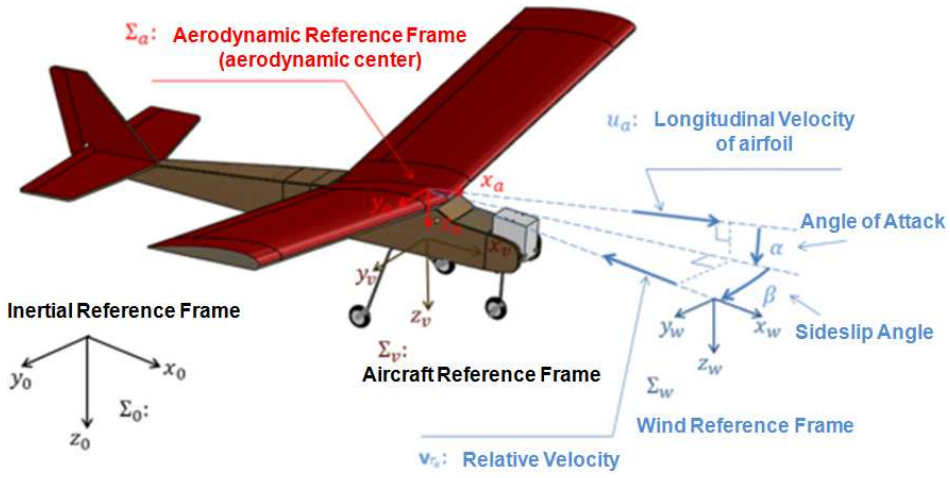

Fig. 1: UAV PT-40 and its reference frames.

II. Background

A. Classical Mechanics

In [5], [6] Lewis and Stengel establish that: the dynamic model of an aircraft regardless of its scale is defined by considering the aircraft as a rigid body. Thus the laws of conservation of momentum (linear and angular momentum) that correspond with the Euler laws of motion can be applied to aircrafts, where in the following equations, (1a)-(1b) are the kinematic ones and (1c)-(1d) are referred to as the Kirchhoff formulation corresponding to the Newton-Euler equations of motion whose 3D elements are expressed with non-inertial frame coordinates [12], [13]:

$$\mathbf{v} = R^T(\boldsymbol{\theta})\dot{\boldsymbol{d}} \quad (1a)$$

$$\boldsymbol{\omega} = R^T(\boldsymbol{\theta})J_\theta(\boldsymbol{\theta})\dot{\boldsymbol{\theta}} \quad (1b)$$

$$\frac{d}{dt}\frac{\partial K}{\partial \mathbf{v}} + \boldsymbol{\omega} \times \frac{\partial K}{\partial \mathbf{v}} = \boldsymbol{f} \quad (1c)$$

$$\frac{d}{dt}\frac{\partial K}{\partial \boldsymbol{\omega}} + \mathbf{v} \times \frac{\partial K}{\partial \mathbf{v}} + \boldsymbol{\omega} \times \frac{\partial K}{\partial \boldsymbol{\omega}} = \boldsymbol{n} \quad (1d)$$

In these equations $\boldsymbol{d} = (x, y, z)^T \in \mathbb{R}^3$ represents the absolute position of the non-inertial reference frame Σ_v, which is rigidly attached to the aircraft, relative to the inertial frame Σ_0; $R(\boldsymbol{\theta}) \in SO(3)$ is the rotation matrix that transforms vector's coordinates from the aircraft reference frame (non-inertial) to the inertial frame; which can be parameterized with the attitude parameters vector $\boldsymbol{\theta} \in \mathbb{R}^m$, for $m = \{3, 4\}$. The matrix operator $J_\theta(\boldsymbol{\theta}) : \mathbb{R}^m \mapsto \mathbb{R}^3$ transforms the rate of change of the orientation vector $\dot{\boldsymbol{\theta}} \mapsto \boldsymbol{\omega}^{(0)}$ to the angular velocity space with inertial coordinates; $\mathbf{v} = (u, v, w)^T \in \mathbb{R}^3$ and $\boldsymbol{\omega} = (p, q, r)^T \in \mathbb{R}^3$ are the linear and angular velocities respectively of the aircraft with local reference frame coordinates. The kinetic energy of the body can be expressed as $K = \frac{1}{2}m\mathbf{v}_c^T\mathbf{v}_c + \frac{1}{2}\boldsymbol{\omega}^T I_c \boldsymbol{\omega}$ where $\mathbf{v}_c = \mathbf{v} + \boldsymbol{\omega} \times \boldsymbol{r}_c$ is the velocity of the center of mass; $\boldsymbol{r}_c \in \mathbb{R}^3$ is the distance from the origin of the local reference frame Σ_v to the center of mass and $I_c = I_c^T > 0 \in \mathbb{R}^{3\times3}$ is the matrix of moments of inertia at the center of mass of the aircraft that is constant in the local reference frame. Finally $\boldsymbol{f} = (f_x, f_y, f_z)^T \in \mathbb{R}^3$ and $\boldsymbol{n} = (n_z, n_y, n_z)^T \in \mathbb{R}^3$ are the external force and torque vectors expressed with local (non-inertial reference frame) coordinates that include the gravity, aerodynamic forces and moments, constraint forces and external disturbances. These forces define the movement of the aircraft in the equations system (1).

In Aeronautics (refer to [5], [6]) the attitude is commonly expressed by the Euler angles roll-pitch-yaw representation, *i.e.* $\boldsymbol{\theta} = (\phi; \theta; \psi)^T$. The corresponding rotation matrix $R(\boldsymbol{\theta}) \in SO(3)$ and the matrix operator $J_\theta(\boldsymbol{\theta})$ used in (1b), using this representation are defined as follows:

$$R(\boldsymbol{\theta}) = \begin{bmatrix} c_\psi c_\theta & -s_\psi c_\phi + c_\psi s_\theta s_\phi & s_\psi s_\phi + c_\psi s_\theta c_\phi \\ s_\psi c_\theta & c_\psi c_\phi + s_\psi s_\theta s_\phi & -c_\psi s_\phi + s_\psi s_\theta c_\phi \\ -s_\theta & c_\theta s_\phi & c_\theta c_\phi \end{bmatrix} \quad (2)$$

$$J_\theta(\boldsymbol{\theta}) = \begin{bmatrix} c_\theta c_\psi & -s_\psi & 0 \\ c_\theta s_\psi & c_\psi & 0 \\ -s_\theta & 0 & 1 \end{bmatrix} \quad (3)$$

where $c_x = \cos(x)$ y $s_y = \sin(y)$.

B. Aerodynamics

Aerodynamic effects arise due to the relative motion between the aerodynamic body i and the wind; these effects are defined by the air-relative velocity vector which is defined with local frame coordinates:

$$\mathbf{v}_{r_i} = \mathbf{v}_{p_i} - R_0^{i\,T}\mathbf{v}_w = \begin{pmatrix} \mathrm{v}_{ri_x} \\ \mathrm{v}_{ri_y} \\ \mathrm{v}_{ri_z} \end{pmatrix}$$

where $R_i \in SO(3)$ is the coordinates transformation (rotation matrix) from the non-inertial reference frame Σ_i attached to the aerodynamic body to inertial frame.

Let be $\bar{c}_i$ and b_i its mean aerodynamic chord and span defined along the main axes x_i and y_i of local frame Σ_i respectively. In Figure 1 the aerodynamic airfoil a is defined. The aerodynamic forces and torques are defined by Lewis in [5] and Roscam in [7] as a function of a set of dimensionless

coefficients as follows:

$$\boldsymbol{f}_{A_i}^{(w_i)} = \bar{q}_i\ S_i \begin{pmatrix} -C_{D_i}(\cdot) \\ C_{Y_i}(\cdot) \\ -C_{L_i}(\cdot) \end{pmatrix} \quad (4)$$

$$\boldsymbol{n}_{A_i}^{(i)} = \bar{q}_i\ S_i \begin{pmatrix} b\ C_{l_i}(\cdot) \\ \bar{c}\ C_{m_i}(\cdot) \\ b\ C_{n_i}(\cdot) \end{pmatrix} \quad (5)$$

where $\boldsymbol{f}_{A_i}^{(w_i)}$ is the aerodynamic forces vector acting on the body i expressed in a virtual reference frame Σ_{wi} given by the air-relative velocity vector (refer to Figure 1); furthermore$\bar{q}_i = \frac{1}{2}\rho\|\mathbf{v}_{r_i}\|$ is the dynamic pressure; S_i is the wing area and ρ is the air density.

On the other hand unlike the vector $\boldsymbol{f}_{A_i}^{(w_i)}$ the aerodynamic torque vector $\boldsymbol{n}_{A_i}^{(i)}$ is expressed in the Σ_i reference frame and its magnitude is weighted by both the mean aerodynamic chord $\bar{c}_i$ and the wingspan b_i.

The magnitude of the aerodynamic coefficients can be determined either experimentally or using a Computational fluid dynamics (CFD) analysis. Their values depend on different variables and geometric characteristics of the airfoils where the aerodynamic angles play an important role; the angle of attack is given by $\alpha_i = \arctan(\mathrm{v}_{ri_z}/\mathrm{v}_{ri_x})$ and the sideslip angle by $\beta_i = \arcsin(\mathrm{v}_{ri_x}/\|\mathbf{v}_{r_i}\|)$. In accordance with Figure 1 there is a rotation matrix $R_{A_i} \in SO(3)$ that transform vectors between the body reference frame and the air-relative reference frame defined by Stengel [6]:

$$R_{A_i}(\alpha_i, \beta_i) = \begin{bmatrix} c_{\alpha_i}c_{\beta_i} & s_{\beta_i} & c_{\beta_i}s_{\alpha_i} \\ -c_{\alpha_i}s_{\beta_i} & c_{\beta_i} & -s_{\alpha_i}s_{\beta_i} \\ -s_{\alpha_i} & 0 & c_{\alpha_i} \end{bmatrix} \quad (6)$$

this matrix allows to express the aerodynamic forces in the local reference frame as follows:

$$\boldsymbol{f}_{A_i}^{(i)} = R_{A_i}^T(\alpha_i, \beta_i)\boldsymbol{f}_{A_i}^{(w_i)} \quad (7)$$

Finally the equations that defined the aerodynamic coefficients C_x in (4)-(5) are presented by Lewis [5] and Stengel [6] as the sum of constant coefficients that are weighted by the aerodynamic variables of the airfoil:

$$C_x = C_{x_0} + \sum_y C_{x_y} \cdot y \quad \forall\ y = \{\alpha, \beta, p, q, r, \delta\}$$

where p, q, r are components of the angular velocity and δ represents the variations of control surfaces that are typically: ailerons, δ_a, elevator δ_e and rudder δ_r in a fixed-wing aircraft.

C. Extended vectors

Let the next vectors be

$$\boldsymbol{\nu}_a^{(i)} = \begin{pmatrix} \mathbf{v}_a^{(i)} \\ \boldsymbol{\omega}_a^{(i)} \end{pmatrix} \in \mathcal{M} \subset \mathbb{R}^6$$

$$\boldsymbol{F}_a^{(i)} = \begin{pmatrix} \boldsymbol{f}_a^{(i)} \\ \boldsymbol{n}_a^{(i)} \end{pmatrix} \in \mathcal{F} \subset \mathbb{R}^6$$

where the extended velocity vector $\boldsymbol{\nu}_a^{(i)} \in \mathbb{R}^6$, or twist, includes the linear velocity of a point a and the angular velocity of the body to which the point belongs, both expressed in an arbitrary reference frame Σ_i; the extended force vector $\boldsymbol{F}_a^{(i)} \in \mathbb{R}^6$, or wrench, includes the forces acting on the point a and the torques acting on the body to which the point belongs, both expressed in the same reference frame Σ_i.

Therefore there are two basic operators defined as extended rotation $\mathcal{R}_j^i$ and extended translation $\mathcal{T}(\boldsymbol{d}_{b/a}^{(i)})$ to transform the extended vectors either between points a and b or between the reference frames Σ_j and Σ_i as follows:

$$\mathcal{T}(\boldsymbol{d}_{b/a}^{(i)}) = \begin{bmatrix} I & -\left[\boldsymbol{d}_{b/a}^{(i)}\times\right] \\ 0 & I \end{bmatrix} \quad (8)$$

$$\mathcal{R}_j^i = \begin{bmatrix} R_j^i & 0 \\ 0 & R_j^i \end{bmatrix} \quad (9)$$

where $\boldsymbol{d}_{b/a} \in \mathbb{R}^3$ is either the distance from point a to point b or the distance from point b to point a; $R_j^i \in SO(3)$ is the rotation matrix that transforms vectors from the reference frame Σ_i to the reference frame Σ_j; $[\boldsymbol{a}\times]$ is the third order skew-symmetric matrix which expresses the 3D vector cross product $[\boldsymbol{a}\times]\boldsymbol{b} = \boldsymbol{a} \times \boldsymbol{b}$ where $(\boldsymbol{a}, \boldsymbol{b}) \in \mathbb{R}^3$.

These operators permit the follow transformations:

$$\boldsymbol{\nu}_b^{(i)} = \mathcal{T}(\boldsymbol{d}_{b/a}^{(i)})\boldsymbol{\nu}_a^{(i)} \qquad \boldsymbol{\nu}_b^{(j)} = \mathcal{R}_j^i\boldsymbol{\nu}_b^{(i)}$$

$$\boldsymbol{F}_b^{(i)} = \mathcal{T}^T(\boldsymbol{d}_{b/a}^{(i)})\boldsymbol{F}_a^{(i)} \qquad \boldsymbol{F}_b^{(j)} = \mathcal{R}_j^i\boldsymbol{F}_b^{(i)}$$

Notice that in order to translate the wrench the extended translation operator defined in (8) needs to be transposed. Thus a new operator can be defined that includes both extended rotation and translation transformations; which in this study is called the Extended Motion Operator (EMO) defined as follows:

$$\mathcal{X}(\boldsymbol{d}_{a/b}, R_j^i) \triangleq \mathcal{R}_j^{i\,T}\mathcal{T}(\boldsymbol{d}_{a/b}^{(j)}) = \mathcal{T}(\boldsymbol{d}_{a/b}^{(i)})\mathcal{R}_j^{i\,T} \quad (10)$$

the EMO directly transforms the extended vectors as shown in the following equations:

$$\boldsymbol{\nu}_a^{(i)} = \mathcal{X}(\boldsymbol{d}_{a/b}, R_j^i)\ \boldsymbol{\nu}_b^{(j)}$$

$$\boldsymbol{F}_a^{(i)} = \mathcal{X}^{-T}(\boldsymbol{d}_{a/b}, R_j^i)\ \boldsymbol{F}_b^{(j)}$$

Finally based on the definition of EMO in (10) and the operators (8)-(9) the following identity can be determined:

$$\dot{\mathcal{X}} = -\Omega(\boldsymbol{\nu}_{a/b}^{(i)})\ \mathcal{X} \quad (11)$$

where the twist $\boldsymbol{\nu}_{a/b}$ is composed of both the relative velocity at point a with respect to point b: $\mathbf{v}_{a/b} = \dot{\boldsymbol{d}}_{a/b}$ and the angular velocity of the reference frame Σ_i with respect to the frame Σ_j: $\boldsymbol{\omega}_{a/b} = \boldsymbol{\omega}_{i/j}$ and $\Omega(\cdot)$ is an operator defined as:

$$\Omega(\boldsymbol{a}) = \begin{bmatrix} [\boldsymbol{a}_2\times] & [\boldsymbol{a}_1\times] \\ 0 & [\boldsymbol{a}_2\times] \end{bmatrix} \in se(3) \quad (12)$$

to an extended vector $\boldsymbol{a} = (\boldsymbol{a}_1^T, \boldsymbol{a}_2^T)^T$.

The operator (10) is defined by Murray in [14] without using the extended rotation and translation operators (8)-(9), the identity (11) is defined using the Lie algebras in $se(3)$ under the condition of screws. It is worth noting that the operator (12) is the equivalent cross product operator for extended vectors which is similar to the cross product operator for 3D vectors $[\boldsymbol{b}\times] \in so(3)$.

III. Dynamic Model

Let $\boldsymbol{q} \in SE(3)$ be the vector that defines the pose (position $\boldsymbol{d} \in \mathbb{R}^3$ and attitude $\boldsymbol{\theta} \in SO(3)$) of the UAV with respect to the inertial reference frame Σ_0; $\boldsymbol{\nu} \in \mathbb{R}^6$ is the extended velocity vector of the UAV expressed in the local (non-inertial) reference frame of the vehicle Σ_v and $\boldsymbol{F} \in \mathbb{R}^6$ the extended exogenous forces vector acting on the UAV expressed also in the local reference frame:

$$\boldsymbol{q} = \left(\boldsymbol{d}^T, \boldsymbol{\theta}^T\right)^T = (x, y, z, \phi, \theta, \psi)^T \quad (13)$$

$$\boldsymbol{\nu} = \left(\mathbf{v}^T, \boldsymbol{\omega}^T\right)^T = (u, v, w, p, q, r)^T \quad (14)$$

$$\boldsymbol{F} = \left(\boldsymbol{f}^T, \boldsymbol{n}^T\right)^T = (f_x, f_y, f_z, n_z, n_y, n_z)^T \quad (15)$$

Thus the kinetic energy can be succinctly expressed as:

$$K = \frac{1}{2}\boldsymbol{\nu}^T M \boldsymbol{\nu} \quad (16)$$

where $M \in \mathbb{R}^{6\times 6}$ is the extended inertia matrix which is constant if it is referenced to a non-inertial reference frame and is defined as follows:

$$M = \begin{bmatrix} mI & -m[\boldsymbol{r}_c\times] \\ m[\boldsymbol{r}_c\times] & I_c - m[\boldsymbol{r}_c\times]^2 \end{bmatrix} = M^T > 0$$

Therefore the system defined by the equations (1) can be rewritten in a simple form as follows:

$$\boldsymbol{\nu} = J_\nu(\boldsymbol{q})\dot{\boldsymbol{q}} \quad (17a)$$

$$\dot{\boldsymbol{P}}(\boldsymbol{\nu}, \dot{\boldsymbol{\nu}}) - \Omega^T(\boldsymbol{\nu})\boldsymbol{P}(\boldsymbol{\nu}) = \boldsymbol{F} \quad (17b)$$

where $\boldsymbol{P}(\boldsymbol{\nu}) = \frac{\partial K}{\partial \boldsymbol{\nu}} = M\boldsymbol{\nu} = (\boldsymbol{p}^T, \boldsymbol{L}^T) \in \mathbb{R}^6$ is the extended momentum vector and $J_\nu \in \mathbb{R}^{6\times 6}$ is a kinematic operator expressed as follows:

$$J_\nu(\boldsymbol{\theta}) = \begin{bmatrix} R^T(\boldsymbol{\theta}) & 0 \\ 0 & R^T(\boldsymbol{\theta})J_\theta(\boldsymbol{\theta}) \end{bmatrix} \quad (18)$$

The wrench of exogenous forces $\boldsymbol{F}$ consist in the addition of the wrench of gravity force $\boldsymbol{F}_g$, the wrench of thrust forces $\boldsymbol{F}_T$ produced by the engines, a restrictive wrench $\boldsymbol{F}_{LG}$ produced by the landing gear, and the wrench of all aerodynamic forces $\boldsymbol{F}_A$ at each of the aerodynamic sections of the aircraft, [9], [10]. All of them expressed with the non-inertial UAV frame coordinates, such that

$$\boldsymbol{F} = \boldsymbol{F}_g + \boldsymbol{F}_T + \boldsymbol{F}_{LG} + \boldsymbol{F}_A$$

The gravity wrench can be computed as $\boldsymbol{F}_g = M\boldsymbol{G}_v$, where the extended gravity vector $\boldsymbol{G}_v = (R^T\boldsymbol{g}_0, 0)^T$ is a coordinates transformation of inertial gravity vector $\boldsymbol{g}_0$ which is defined according to the inertial frame definition attached to the Earth.

The general thrust wrench is defined by both a longitudinal force and a load torque; its magnitude depends on the characteristics of the motor/propeller and can be computed as $\boldsymbol{F}_{T_n} = (T, 0, 0, n_T, 0, 0)^T$ where T is the longitudinal thrust and n_T is the load torque produced by the spinning of the propeller. The total thrust wrench (equation (19b)) is the sum of effects produced by the n Powerplants on the UAV expressed in the non-inertial reference frame. The equation (19) presents the EMO $\mathcal{X}_{T_n}$ which transforms vectors between the non-inertial reference frame and the frame attached to the engine where $\boldsymbol{r}_{T_n}$ is the distance between the reference frames and ϑ represent the orientation of the motor with respect to the non-inertial reference frame of the aircraft.

$$\mathcal{X}_{T_n} = \mathcal{X}(\boldsymbol{r}_{T_n}, R_v^{T_n}(\vartheta)) \quad (19a)$$

$$\boldsymbol{F}_T = \sum_n \mathcal{X}_{T_n}^T \boldsymbol{F}_{T_n} \quad (19b)$$

The force produced by the landing gear consist in the sum of the constraint components arising from the j independent constraint points of the landing gear with the ground:

$$\boldsymbol{F}_{LG} = \sum_j \mathcal{X}_{LG_i}^T \boldsymbol{F}_{LG_j}^{(0)}(\boldsymbol{r}_{LG_j}, R(\boldsymbol{\theta}), \boldsymbol{\nu}_{LG_j}^{(0)}) \quad (20)$$

where the constraint forces in the wheels $\boldsymbol{F}_{LG_j}^{(0)}$ are expressed with inertial frame coordinates and they are active only during landing and take off. The twist $\boldsymbol{\nu}_{LG_j}^{(0)} = \mathcal{X}_{LG_j}\boldsymbol{\nu}$ represents the extended velocity vector of the UAV expressed in an auxiliar reference frame on each wheel, where $X_{LG_j}(\boldsymbol{r}_{LG_j}, R(\boldsymbol{\theta}))$ is the EMO which transform between reference frames and $\boldsymbol{r}_{LG_j}$ is the distance between each wheel and the non-inertial frame of the airship.

The aerodynamic wrench can be computed as the sum of the i aerodynamic wrenches $\boldsymbol{F}_{A_i}$, equation (21b), acting on each component of the UAV; hence there is an extended motion operator $\mathcal{X}_i$ for each aerodynamic section that expresses the position $\boldsymbol{r_i} \in \mathbb{R}^3$ of the aerodynamic center of the i^{th} component and the relative attitude of this element with respect to the non-inertial reference frame rigidly attached to the UAV $R_v^i(\varphi_i, \bar{\alpha}_i) \in SO(3)$, which is produced by both the dihedral φ_i angle and the angle of incidence $\bar{\alpha}_i$ in the design and installation of each airfoil.

$$\mathcal{X}_i = \mathcal{X}(\boldsymbol{r}_i, R_v^i(\varphi_i, \bar{\alpha}_i)) \quad (21a)$$

$$\boldsymbol{F}_A = \sum_i \mathcal{X}_i^T \boldsymbol{F}_{A_i}^i(\boldsymbol{\nu}_{r_i}^i) \quad (21b)$$

Notice that the elements of the aerodynamic wrench $\boldsymbol{F}_{A_i}(\boldsymbol{\nu}_{r_i}) = (\boldsymbol{f}_{A_i}^T, \boldsymbol{n}_{A_i}^T)^T$ are calculated by (5)-(7); on the other hand the relative velocity twist of each section $\boldsymbol{\nu}_{r_i}^i$ which is necessary to determined the aerodynamic wrench is calculated as follows:

$$\boldsymbol{\nu}_{r_i} = \mathcal{X}\boldsymbol{\nu} - \mathcal{R}_0^{i\,T}\boldsymbol{\nu}_w^{(0)} \quad (22)$$

where $\mathcal{R}_0^i = \mathcal{R}_0^v\mathcal{R}_v^i$.

This consideration implies that each section has an angle of attack α_i, a sideslip angle β_i and a control surface which correspond at the ailerons δ_{ai}, elevator δ_e and ruder δ_r.

IV. Case Study

PT-40 of *Great Planes*® is considered as a case study here (refer to figure 1). The reference frame Σ_v is rigidly attached in the center of mass, *i.e.* $\boldsymbol{r}_c = 0$, and its parameters both geometric and dynamic are presented in the table I. The rotation of the propeller produces a load torque that creates induced roll moment on the airplane. This moment is neglected in many cases either because its effects are not significants or because the wing resist the rolling motion.

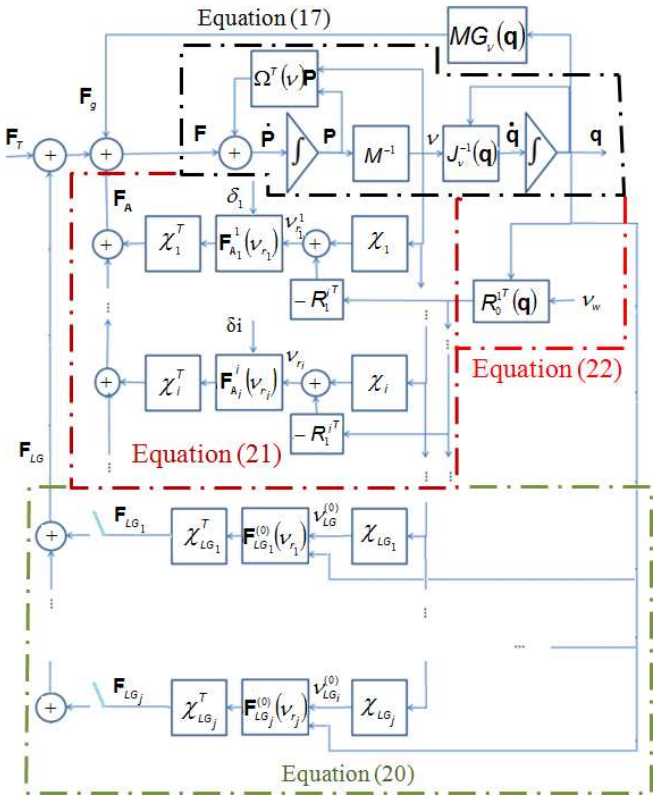

Fig. 2: General schematic of the dynamic model of PT-40 aircraft. This schematic considers the aerodynamic wrench as the sum of each independent effect.

TABLE I: Geometric and dynamic parameters of PT-40.

Parameter	Value	Parameter	Value
m	$2.26\ (kg)$	$I_{xx}(kg\ m^2)$	0.151
b	$0.985\ (m)$	$I_{yy}(kg\ m^2)$	0.173
S	$0.435\ (m^2)$	$I_{zz}(kg\ m^2)$	0.293
$\bar{c}$	$0.286\ (m)$	$I_{xz}(kg\ m^2)$	0.0031

Roscam in [7] defines that it is not possible neglects these effects in all cases because these depends of the number of propellers, its moment of inertia and their angular velocity. In this paper a formal Thrust Model is not presented and the load torque of the propeller is not considered; thus the thrust wrench, called simply thrust, produced by the propeller is considered to acts in the longitudinal direction of the PT-40, this means that thrust is parallel to the x axis and belongs to the reference frame Σ_v.
The thrust wrench is defined as:

$$\boldsymbol{F}_T = (T, 0, 0, 0, 0, 0)^T \tag{23}$$

The aerodynamic coefficients are calculated considering two wing sections and the empennage (vertical and horizontal stabilizers) which included the surface control (ailerons, elevator and rudder). The aerodynamic contributions of the fuselage are not considered in this study because these are not important for the performance of a fixed wing airplane with a small angle of attack [6]. Furthermore, for aircrafts with an aspect ratio higher than 5, $AR = b_i^2/S_i > 5$, the lift produced by the wing is approximately equal to the combination wing-fuselage [7], however these can be included.

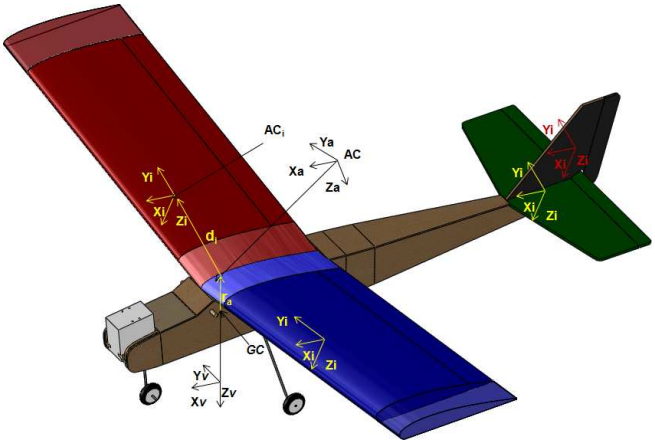

Fig. 3: Aerodynamic sections of the PT-40.

Two approaches are presented in this work: the traditional approach (lumped aerodynamic parameters which correspond to an equivalent aerodynamic section) and the sectional approach (lumped aerodynamic parameters on each section). The aerodynamic coefficients are calculated off line using TORNADO software [15] that considers the vortex lattice method and potential flow.

A. *Traditional approach*

Roscam, Stengel and Lewis define both the total aerodynamic forces and torques as the sum of the aerodynamic effects on each component of the airplane. However some of these effects are neglected when they have no significant effects with respect to the wing effects or in order to simplify the mathematical operations [7] [8].

TABLE II: Aerodynamic coefficients for traditional approach.

Coefficient	Value	Coefficient	Value
C_{L_0}	0.30317	$C_{l_{\delta_e}}$	0.408081
C_{D_0}	0.0060332	$C_{D_{\delta_e}}$	0.00358
C_{L_α}	4.463	$C_{Y_{\delta_a}}$	$-2.8111e^{-9}$
C_{L_q}	8.463	$C_{Y_{\delta_r}}$	-0.076306
C_{D_α}	0.14974	$C_{n_{\delta_r}}$	-0.04363
C_{D_q}	0.18712	C_{l_β}	0.10872
C_{Y_β}	-0.24134	$C_{l_{\delta_r}}$	-0.00120
C_{Y_p}	0.24052	C_{l_p}	-0.4378
C_{m_α}	-1.3041	$C_{m_{\delta_e}}$	-1.07276
C_{m_q}	-11.9563	C_{l_r}	0.0526
C_{n_β}	-0.093892	C_{l_β}	0.10872
C_{n_p}	0.027599	$C_{n_{\delta_a}}$	$-1.352e^{-9}$
C_{n_r}	-0.10273	C_{Y_r}	-0.21941
C_{m_0}	0.024965	C_{D_q}	0.18712
$C_{L_{\delta_e}}$	0.408081	$C_{n_{\delta_e}}$	0
$C_{Y_{\delta_e}}$	0		

The traditional approach considers the movement of both ailerons through an angle δ_a as well as the movements of the elevator and rudder through δ_e and δ_r respectively. This approach also considers a single reference frame Σ_a which is

rigidly attached to the PT-40 in the aerodynamic center of the wing where the aerodynamic effects are concentrated (refer to Figure 1). It is noteworthy that the aerodynamic analysis for the traditional approach considered the geometry of the aircraft as a whole body where the dihedral angle and the angle of incidence of each component are included. Table II presents the aerodynamic coefficients of the PT-40 for traditional approach.

B. Sectional approach

This approach considers four sections which are defined as: two wing segments, a vertical stabilizer and a horizontal stabilizer. Refer to Figure 3 to identify the component of the PT-40. Each section is analyzed and its aerodynamic coefficients are calculated (in Tables III-V the aerodynamic coefficients are presented). The wing of the PT-40 has a dihedral angle $\varphi = 9.5^\circ$ that improves lateral stability. Furthermore, the wing has an angle of incidence $\bar{\alpha} = 3^\circ$ that defines the deviation of the chord from the longitudinal axis of the non-inertial frame in the center of mass and the horizontal stabilizer has an angle of incidence $\bar{\alpha} = -2^\circ$.

TABLE III: Aerodynamic coefficients of horizontal stabilizer in accordance with the sectional approach.

Coefficient	Value	Coefficient	Value
C_{L_0}	0	$C_{l_{\delta_e}}$	0
C_{D_0}	0	$C_{D_{\delta_e}}$	$2.6e^{-5}$
C_{L_α}	3.6856	$C_{Y_{\delta_a}}$	0
C_{L_q}	3.8108	$C_{Y_{\delta_r}}$	0
C_{D_α}	$1.1300e^{-4}$	$C_{n_{\delta_r}}$	0
C_{D_q}	$1.0e^{-6}$	C_{l_β}	0
C_{Y_β}	0	$C_{l_{\delta_r}}$	0
C_{Y_p}	0	C_{l_p}	-0.3526
C_{m_α}	$7.7178e^{-2}$	$C_{m_{\delta_e}}$	-0.5363
C_{m_q}	-0.6796	C_{l_r}	0
C_{n_β}	0	$C_{l_{\delta_a}}$	0
C_{n_p}	0	$C_{n_{\delta_a}}$	0
C_{n_r}	0	C_{Y_r}	0
C_{m_0}	0	C_{D_q}	$1e^{-6}$
$C_{L_{\delta_e}}$	1.8038	$C_{n_{\delta_e}}$	0
$C_{Y_{\delta_e}}$	0		

V. Simulation results

The stability of aerial vehicles, either UAVs or traditional airplanes, can be analyzed by uncoupling the dynamic model in two general modes of aircraft motions which are called longitudinal and lateral-directional motions. These modes of motions arise from the linearization of a nonlinear dynamic model of the airplane which depends on the predominant aerodynamic coefficients. Refer to [5], [6], [7], [16]. The linear model of longitudinal motion establishes that: the longitudinal and vertical linear velocities u and w respectively, the component of the angular velocity q and the pitch angle θ have to present asymptotic behavior either with or without perturbation forces. The linear model of lateral-directional motion defines the movements of the aerial vehicle in both the y and z axes; these movements are developed out of the plane of symmetry and are coupled with the longitudinal motion because of the nonlinear aerodynamic effects, but

TABLE IV: Aerodynamic coefficients of wing section accordance with the sectional approach.

Coefficient	Value	Coefficient	Value
C_{L_0}	$9.4988e^{-2}$	$C_{l_{\delta_e}}$	$1.799e^{-3}$
C_{D_0}	$9.3e^{-4}$	$C_{D_{\delta_e}}$	$2.0436e^{-2}$
C_{L_α}	3.1849	$C_{Y_{\delta_a}}$	0
C_{L_q}	3.3309	$C_{Y_{\delta_r}}$	0
C_{D_α}	$6.3854e^{-2}$	$C_{n_{\delta_r}}$	0
C_{D_q}	$6.6351e^{-2}$	C_{l_β}	0
C_{Y_β}	0	$C_{l_{\delta_r}}$	0
C_{Y_p}	0	C_{l_p}	-0.2573
C_{m_α}	$7.3695e^{-2}$	$C_{m_{\delta_e}}$	-0.37875
C_{m_q}	$-6.2862e^{-1}$	C_{l_r}	$1.016e^{-2}$
C_{n_β}	0	$C_{l_{\delta_a}}$	0
C_{n_p}	$1.184e^{-2}$	$C_{n_{\delta_a}}$	0
C_{n_r}	$-3.62e^{-4}$	C_{Y_r}	0
C_{m_0}	$-3.5e^{-2}$	C_{D_q}	$6.6351e^{-2}$
$C_{L_{\delta_e}}$	1.1238	$C_{n_{\delta_e}}$	$-4.4e^{-5}$
$C_{Y_{\delta_e}}$	0		

TABLE V: Aerodynamic coefficients of vertical stabilizer accordance with the sectional approach.

Coefficient	Value	Coefficient	Value
C_{L_0}	0	$C_{l_{\delta_e}}$	0.064457
C_{D_0}	0	$C_{D_{\delta_e}}$	$2.5584e^{-5}$
C_{L_α}	1.827	$C_{Y_{\delta_a}}$	0
C_{L_q}	2.1818	$C_{Y_{\delta_r}}$	0
C_{D_α}	$7.9102e^{-5}$	$C_{n_{\delta_r}}$	0
C_{D_q}	0	C_{l_β}	0
C_{Y_β}	0	$C_{l_{\delta_r}}$	0
C_{Y_p}	0	C_{l_p}	-0.1610
C_{m_α}	-0.067067	$C_{m_{\delta_e}}$	-0.4665
C_{m_q}	-0.7105	C_{l_r}	0
C_{n_β}	0	$C_{l_{\delta_a}}$	0
C_{n_p}	0	$C_{n_{\delta_a}}$	0
C_{n_r}	0	C_{Y_r}	0
C_{m_0}	0	C_{D_q}	0
$C_{L_{\delta_e}}$	1.0366	$C_{n_{\delta_e}}$	$-5.4767e^{-6}$
$C_{Y_{\delta_e}}$	$-8.3882e^{-6}$		

these (the longitudinal motion) do not perturb the lateral-directional motion. In order to achieve either longitudinal or lateral-directional stability, the torques around the axes of the non-inertial frame must be canceled. The dihedral angle of the PT-40 improves lateral stability because it has a strong influence on the roll moment. On the other hand the vertical stabilizer aligns the airplane with the relative wind velocity. By canceling the torques the angular acceleration decreases and the angular velocities p and r present asymptotic behavior.

The dynamic model of PT-40 is not linearized and is analyzed under specific conditions in order to verify the complete behavior of the vehicle. A comparison between the traditional and sectional approaches of the aerodynamic effects is presented in this paper; Figure 2 presents a block diagram of the dynamic model including the exogenous wrenches. The test conditions are defined as follows: The time period $t = [0 - 60]sec$ corresponds to the take-off stage where perturbation effects are not included; the period of time $t = [60 - 65]sec$ corresponds to a longitudinal wind flow disturbance with a magnitude of 2 m/s at -10° from

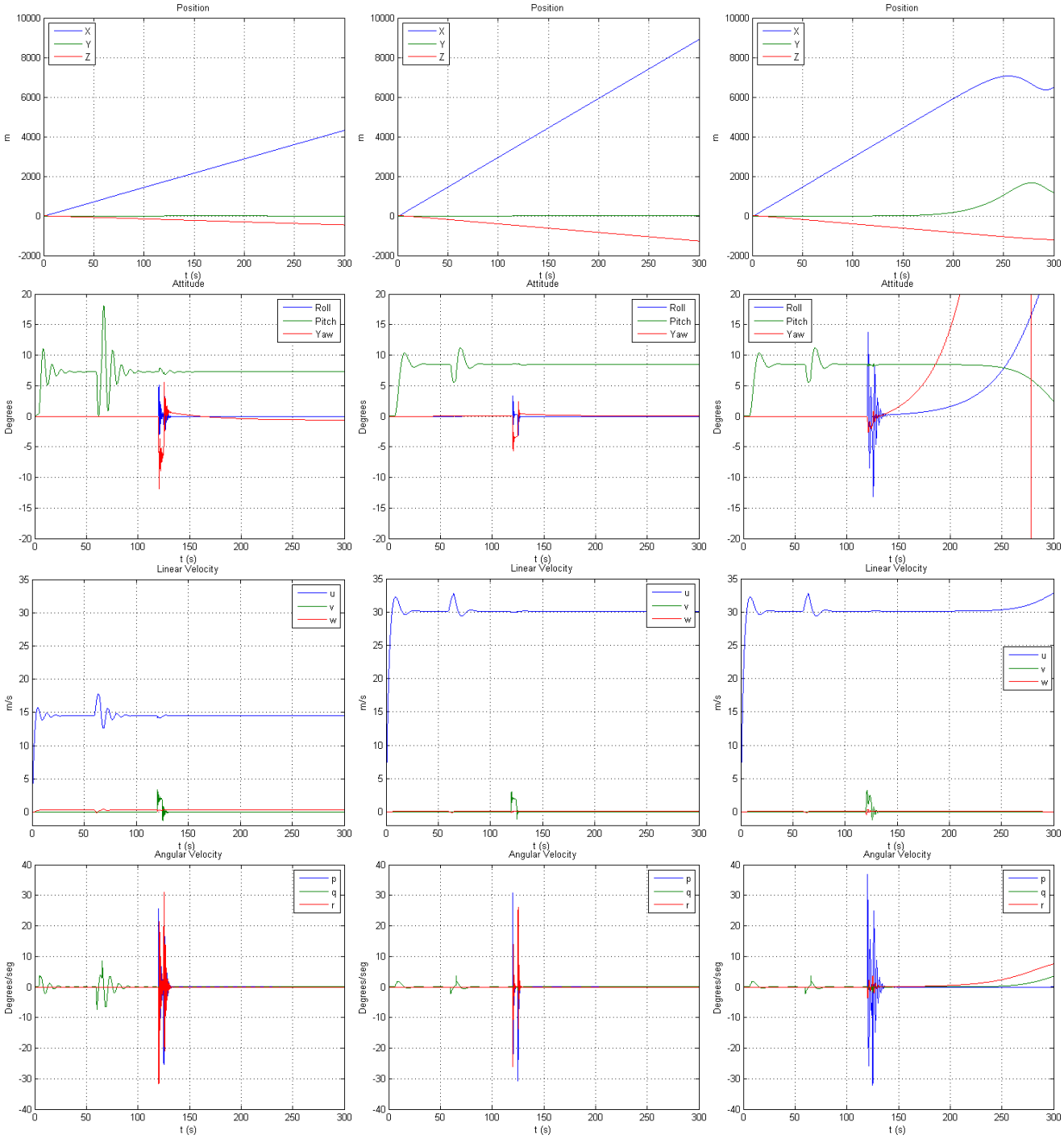

Fig. 4: Open-loop state variables results for traditional approach (left column), sectional approach (center column) and sectional approach without vertical stabilizer (right column). From top to bottom: inertial position $\boldsymbol{d}$ (first row), attitude roll-pitch-yaw Euler angles $\boldsymbol{\theta}$ (second row), linear velocity $\mathbf{v}$ (third row), and angular velocity $\boldsymbol{\omega}$ (bottom row).

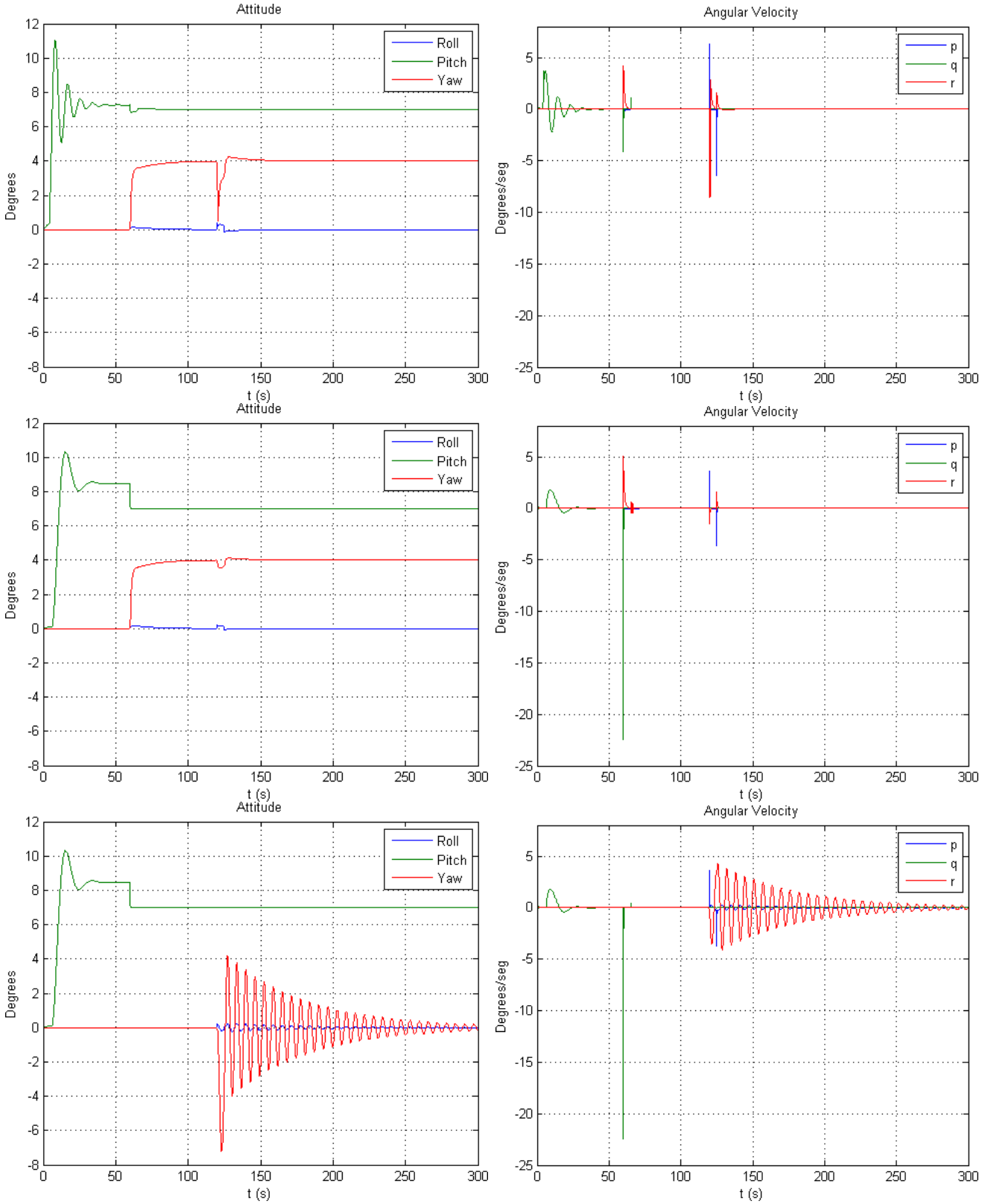

Fig. 5: PD closed-loop results for traditional approach (row above), sectional approach (center row) and sectional approach without vertical stabilizer case 3 (row below). From left to right: Attitude $\boldsymbol{\theta}$ and Angular velocity $\boldsymbol{\omega}$.

the inertial axis; finally in the time period $t = [120-125]sec$ a lateral wind flow disturbance with a magnitude of 2 m/s and 90° from the $x_0 - z_0$ axes is included. The above test conditions are used to analyze the PT-40 considering the following cases:

1) traditional approach

2) sectional approach

3) sectional approach without vertical stabilizer

The restrictive wrench $\boldsymbol{F}_{LG}$ due to the floor, one for each wheel, is considered in this model in order to simulate the take-off. Their effects are expressed in the inertial reference frame and are modeled as a Mass-Spring-Damper system where their effects act in the vertical direction. In addition, the thrust wrench $\boldsymbol{F}_T$ induced by the propeller is defined as $T = T_0(1 - 0.7|u|)$; this equation retrieves the effects of induced velocity where T_0 is the initial thrust.

A. Open-loop behavior

Figure 4 presents the evolution of the state variables of the aircraft, defined by the position, attitude, linear velocity and angular velocity for the three defined cases. In all cases the asymptotic behavior of the longitudinal stability that is described in the literature is presented; the initial thrust T_0 for take-off in both the second and third cases are higher than the first case. The sectional approach needs 80% additional initial thrust with respect to the traditional approach. This difference is due to the effects of pressure distribution in the aerodynamic analysis of the PT-40 based on the sectional approach. The position vector presents the same qualitative behavior in both the first and second cases, however the difference is the slope presented by the displacement along the x_0 inertial axis. This behavior is due to the thrust magnitude that is applied in this approach. In the time period $t = [0 - 120]sec$ the angles ϕ and ψ, which are components of the attitude vector $\boldsymbol{\theta}$, are null because there are no lateral forces or nonlinear affects that perturb the lateral-directional stability. The PT-40 increases its velocity and thus the aerodynamic wrench $\boldsymbol{F}_A$ increases its value until it exceeds the gravity wrench and θ increases starting the take-off phase. However, despite the fact that all the cases present asymptotic longitudinal behavior, the first case presents important oscillations. The angular velocity vector exhibits the same behavior described where p and r are null and q converges to a steady state when θ achieves stability.

The longitudinal wind flow disturbance during $t = [60 - 65]sec$ affects the longitudinal stability and the variables θ, q, u and w converge asymptotically. However the oscillations present in the first case, the traditional approach, have greater amplitude. Moreover the sectional approach requires less time to stabilize. Notice that the perturbations in the longitudinal plane do not affect the lateral-directional stability.

The lateral wind flow disturbance in the time period $t = [120 - 125]$ affects both the longitudinal and the lateral-directional motion (refer to Figure 4). The lateral stability is achieved when both ϕ and p converge to zero. This behavior is produced by the dihedral angles of the wing because this angle affects the rolling moment and the sideslip angle. The directional stability is guaranteed because of the behavior of the variables ψ and r where ψ starts to diverge until the PT-40 is aligned with the relative velocity. Furthermore r converges to a steady state after the wind flow disturbance; based on the results, the lateral-directional stability of the PT-40 is guaranteed for the first and second cases. The PT-40 in the third case achieves longitudinal stability but due to the absence of the vertical stabilizer both the directional and lateral stability of the PT-40 fail; this behavior occurs because there is no restoring force that forces the PT-40 to align with the relative velocity. These results demonstrate the importance of the vertical stabilizer for the stability of any aerial vehicle with traditional configuration.

B. Close-loop behavior

In order to study the behavior of the dynamic model a simple PD attitude control is implemented for the roll, pitch and heading variables independently; where the values of the feedback gains, tuned empirically using the numerical simulator are shown in Table VI. The result for reference set point signals at 0° Roll, 7° Pitch and 4° Yaw are presented in Figure 5. First and second cases converge to the signal references even in the presence of disturbing forces. In the third case, due to the absence of vertical stabilizer and then of rudder the PT-40 cannot achieve directional (yaw) stability and requires more time to achieve lateral (roll) stability in the presence of disturbing forces. This result suggest that directional stability is influenced by both, the dihedral angle and ailerons, which is the known effect that the directional angle ψ can be modified using roll angle ϕ, even the absence of the vertical stabilizer.

TABLE VI: Feedback gains

Control	P-gain	D-gain
Roll	8	0.3
Pitch	11	0.5
Yaw	10	9

C. Independent ailerons

The sectional approach allows to modify the angular displacement of each aileron in both extremes of the wing independently. Two cases have been considered. 1) An open-loop simulation under the following conditions. First in the time period $t = [40-50]sec$ both ailerons (flap-like motion) are moved upward $\delta_a = 5^\circ$. Then at $t = [90-100]sec$ both ailerons are moved downward $\delta_a = -5^\circ$. Next in the time interval $t = [140 - 145]sec$ ailerons are moved in opposite direction (aileron-like motion) with $\delta_a = 0.5^\circ$ where the right aileron is moved upward. Finally at $t = [190-195]sec$ both ailerons are moved in opposite directions of its previous values. 2) A similar simulation to the previous case with two different changes. First a pitch control is included and second the aileron angles on the first and the second time periods (flap-like motion) has been modified to 30°. In Figure 6 there are shown the pose curves of the first case while on Figure 7 there are shown the results of the second case.

Open-loop simulation (Figure 6) shows that both the wing lift force and the pitch torque decrease due to the

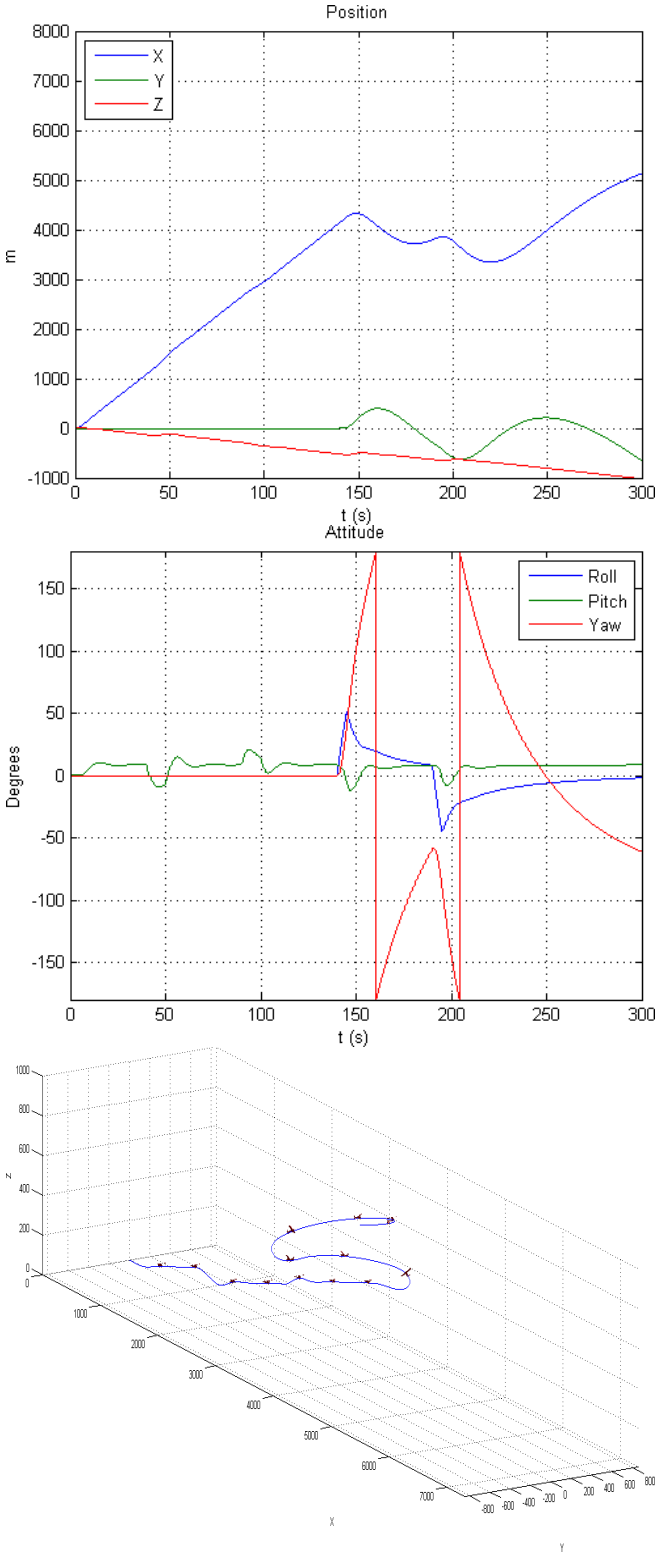

Fig. 6: Open-loop behavior in all control surfaces with different combination independent movements of the ailerons.

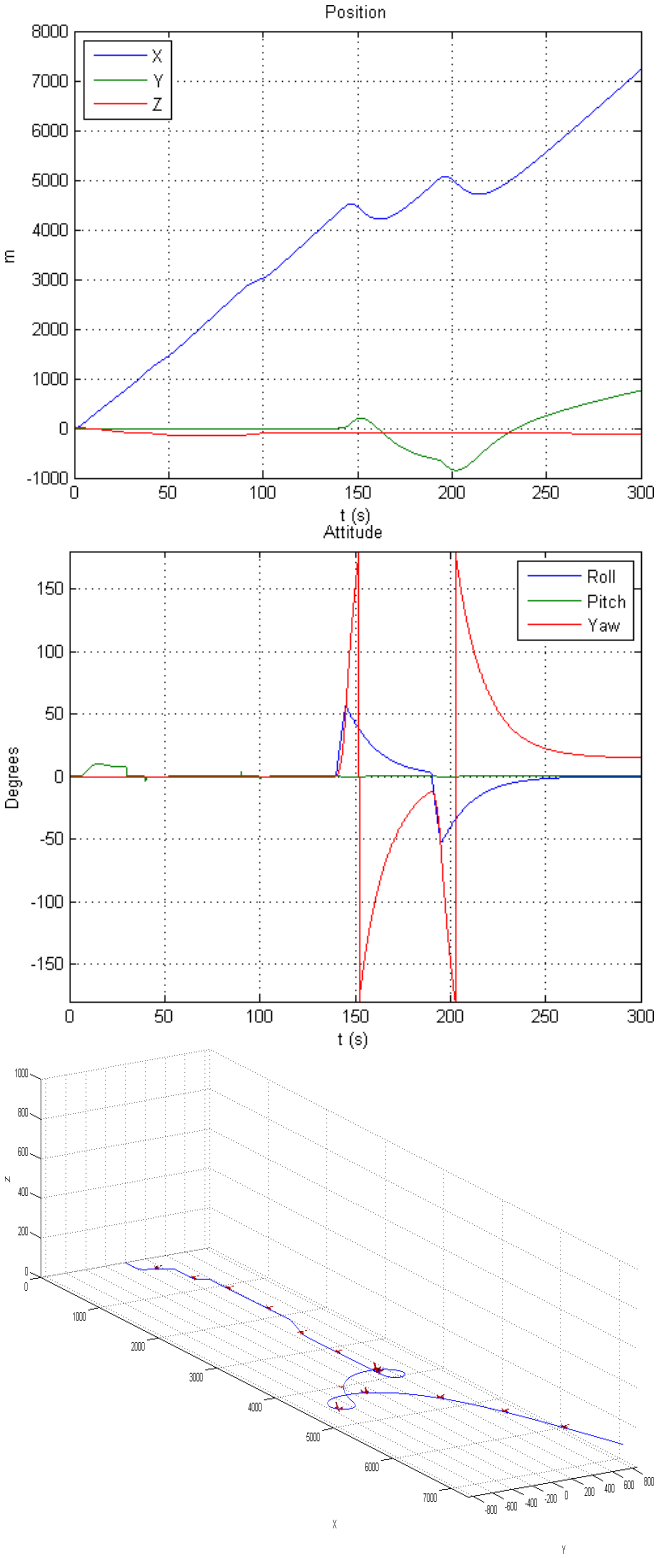

Fig. 7: Open-loop behavior in the aileron with different combination during different time periods and a close-loop behavior for the pitch angle.

upward position of the ailerons; therefore the PT-40 nose goes down and the slope of the displacement along the z_0 decreases. In the second time period the downward position of both ailerons increase the slope of the vertical displacement because of the components of the aerodynamic wrench increases. It is noteworthy that this behavior correspond to the basic aerodynamic characteristics of an airfoil with

a control surface. The basic functions of the ailerons are recovered when they are moved in a opposite way as is presented in the second two time periods: the first of them (the third overall time period) shows that banking motion to the right that reach almost 50° in a very short time and which decreases due to the dihedral induced longitudinal stability until the last period induce the opposite rolling motion. In this third period, the heading angle diverges and the aircraft turns until approximately 300° around its vertical axis, furthermore the pitch angle θ decreases because of the high value of the roll angle ϕ and the PT-40 decrease its altitude. Finally, in the last time period presents a similar behavior to the previous period with an important change in the magnitude of the heading divergence which rises to than 360° from the previous initial orientation. Notice also the changes in the slopes of the position curves in the first row as well as the trajectory path in the third row (path drawing based on [17]).

For the case with pitch control, the aileron angle is increased to 30° in both flap-like motion periods because the torque produced by the horizontal stabilizer due to the pitch control cancels the total torque produced by the upward and downward position of the ailerons, Figure 7. Notice that due to the pitch control, the banking motion to both sides tends to be more symmetric, that is in both cases the aircraft almost performs a the complete horizontal loop in both directions, with a maximum banking angle of about 50°.

It is noteworthy that according with the tables III and IV the coefficients $C_{L_{\delta_e}}$ and $C_{m_{\delta_e}}$ (variation of airplane lift and pitch moment coefficients with control surface deflection angle) are similar in both airfoil sections. Then considering the relationship between horizontal stabilizer and wing areas $\frac{A_{HE}}{A_{wing}} \approx 42\%$ the torque produced by the horizontal stabilizer is dominant because of the lever arm between the aerodynamic center of the stabilizer and the center of mass of the airship. However the effectiveness of ailerons can be improved by increasing their chord line (the chord line of ailerons in the PT-40 represents 10% of the wing chord).

Based on the results in the Figure 6 the basic functions of the ailerons and their effects are recovered because the opposite movement of the ailerons produced changes in the roll and yaw attitude, furthermore these results suggest that the combination of the elevator with the independent positioning of the ailerons can improve the behavior of the PT-40; e.g., change the rate of climb of the PT-40 and facilitate the rapid recovery of its attitude.

VI. Conclusions

The general sectioning aerodynamic modeling for aerial vehicles using extended vectors, which can be applied to any traditional aircraft, UAV or morphing UAV regardless of their size, is presented in this paper. The dynamic model is expressed as functions of the extended momentum vector $\boldsymbol{P}$ and the Ω operator. This representation facilitates the numerical implementation and therefore permits any wrench that represents exogenous forces and moments to be included, such as the aerodynamic or restrictive effects, by applying the appropriated transformations. This representation expresses the mathematical model in a simple way and facilitates the implementation for numerical simulation. The aerodynamic sectional approach in conjunction with the Extended Motion Operator EMO enables effects that are otherwise impossible to be include or implement in the traditional approach such as the independent positioning of the ailerons, the dihedral and incidence angles of the wing, and the position and attitude of any airfold component that is subject to kinematic changes, resulting in a simple method of analysis and design for aerial vehicles and morphing systems. Although the quantitative values for the aerodynamic forces/torques need to be adjusted because of the continuity of the dynamic pressure along the span of the airfold sections, the sectional approach proves to be a promising tool for the modeling of complex aerial vehicles/systems.

Acknowledgements

This work was partially supported by PROMEP.

References

[1] H. Castañeda, J. de León-Morales, and E. Olguín-Díaz, "Path tracking of a fixed-wing autonomous aerial vehicle by high order sliding mode control," *Proccedings of ASME International Design Engeneering Technical Conferences and Computers and Information in Engineering Conference, Whasington D.C. USA*, 2011.

[2] J. Gerdes and S.-K. Gupta, "Design, analysis, and testing of a flapping wing miniature air vehicle," Master of Science, Department of Mechanical Engineering, Institute for Systems Research University of Maryland, 2010.

[3] J. Grauer and J. Hubbard, "Modeling of ornithopter flight dynamics for state estimation and control," *American Control Conference. Marriott Waterfront, Baltimore, MD, USA*, June-July 2010.

[4] A.-A. Paranjape, J. Kim, and S. jo Chung, "Closed-loop perching of aerial robots with articulated flapping wings," *IEEE*, 2012.

[5] B. Stevens and F. L. Lewis, *Aircraft control and simulation*, 2nd ed. John Wiley & sons, Inc., 2003.

[6] R. Stengel, *Flight Dynamics*. Princeton University press, 2004.

[7] J. Roscam, *Airplane flight dynamic and automatic flight control*, 6th ed. DARcorporation, 2003.

[8] T. Cheviron, A. Chriette, and F. Plestan, "Generic nonlinear model of reduced scale uavs," *IEEE International Conference on Robotics and Automation*, pp. 3271–3276, May 2009.

[9] A. Noth, "Design of solar powered airplanes for continuous flight," Ph.D. dissertation, Swiss Federal Institute of technology Zurich, September 2008.

[10] A.-A. Paranjape, S.-J. Chung, and M. S. Lelig, "Flight mechanics of a tailless articulated wing aircraft," *Bioinspiration & Biomimetic*, 2011.

[11] R. Featherstone, *Rigid Body Dynamics Algorithms*, Springer, Ed., 2008.

[12] L. Meirovitch, *Methods of analytical dynamics*. Courier Dover Publications, 1970.

[13] T.-I. Fossen and O.-E. Fjellstad, "Nonlinear modellinig of marine vehicles in 6 degrees of freedom," *Journal of Mathematical Modelling of systems*, vol. 1, no. 1, 1995.

[14] R. Murray and L. Zexiang, *A Mathematical Introduction to Robotic Manipulation*. CRC Press, 1994.

[15] T. Melin, "A vortex lattice matlab implementation for linear aerodynamic wing applications," Master's thesis, Royal Institute of Technology (KTH), Department of aeronautics, December 2000.

[16] M.-V. Cook, *Flight Dynamics Principles*, 2nd ed. ELSEVIER, 2007.

[17] V. Scordamaglia, "Trajectory and attitude plot version 3," MatlabCentral in http://www.mathworks.com/matlabcentral/fileexchange/5656-trajectory-and-attitude-plot-version-3/content/trajectory3.m, August 2004.